First-principles prediction of electron grain boundary scattering in FCC metals

Tianji Zhou, Atharv Jog, and Daniel Gall

Department of Materials Science and Engineering, Rensselaer Polytechnic Institute, Troy, New York 12180, USA

Abstract

The electron reflection probability r at symmetric twin boundaries $\Sigma 3$, $\Sigma 5$, $\Sigma 9$ and $\Sigma 11$ is predicted from first principles for the eight most conductive face-centered cubic (fcc) metals. r increases with decreasing interplanar distance of atomic planes parallel to the boundary. This provides the basis for an extrapolation scheme to estimate the reflection probability r_r at random grain boundaries which is relatively small, $r_r = 0.28$ -0.39, for Cu, Ag, and Au due to their nearly spherical Fermi surfaces, but approximately two times higher for Al, Ca, Ni, Rh, and Ir with a predicted $r_r = 0.61$ -0.72. The metal resistivity in the limit of small randomly oriented grains with fixed average size is expected to be proportional to the materials benchmark quantity $\rho_0 \lambda \times r_r/(1-r_r)$, where ρ_0 and λ are the bulk resistivity and bulk electron mean free path. Cu has the lowest value for this quantity, indicating that all other fcc metals have a higher resistivity in the limit of small randomly oriented grains. Thus, the conductivity benefit of replacement metals for narrow Cu interconnect lines can only be realized if the grains are larger than the line width or exhibit symmetric orientation relationships where $r < r_r$.

The electrical resistivity ρ of polycrystalline metals increases with decreasing average grain size D. This resistivity size effect has been a topic of research for multiple decades but has recently gained considerable attention because the resistance of interconnect wires in integrated circuits causes signal delay and power consumption that limits continued device downscaling. The resistivity increase in interconnects is attributed to both electron scattering at surfaces and grain boundaries. In this letter, we focus on the latter, which becomes dominant if the grain size is reduced to below the bulk electron mean free path λ which is, for example, 39 nm for copper at room temperature. Multiple metals have been proposed as Cu replacement options for interconnects because they have smaller λ values and may therefore exhibit a less pronounced resistivity increase. Because they have smaller λ values and may therefore exhibit a less pronounced resistivity increase. However, the resistivity contribution from grain boundary scattering is also affected by the electron reflection probability, as described by the classical model by Mayadas and Shatzkes (MS). An approximate form of the MS-model predicts the resistivity ρ of a polycrystalline metal to increase with decreasing average grain size D according to:

$$\rho = \rho_o \left[1 + \frac{3}{2} \frac{R}{1 - R} \frac{\lambda}{D} \right],\tag{1}$$

where ρ_0 is the bulk resistivity and R is an effective mean reflection probability at the grain boundaries. Eq. (1) indicates that grain boundaries cause an additive contribution to the resistivity $\rho_{\rm gb} = 1.5 \times \rho_0 \lambda/D \times R/(1-R)$ and that the resistivity contribution from grain boundaries is therefore proportional to the material parameter $\rho_0 \lambda \times R/(1-R)$. We propose to use this parameter as a

descriptor to search for interconnect metals because the metal with the smallest $\rho_o \lambda \times R/(1-R)$ is most conductive in the limit of a small but fixed grain size. The pre-factor $\rho_o \lambda$ has been the focus of multiple studies which compare the $\rho_o \lambda$ product for different conductors to evaluate their potential for narrow high-conductivity wires. ^{16,32,38,39} In contrast, much less is known about the grain boundary reflection coefficient R, which is similarly important in predicting promising metals for narrow interconnects. ^{32,40–44}

Measurements of the grain boundary reflection probability is challenging because $\rho_{\rm gb}$ depends on the grain orientation distribution^{25,45} which is affected by the materials synthesis process. $^{46-48}$ As a result, R is commonly used as an empirical parameter which is obtained from fitting experimental data with Eq.(1). 35,36,49-54 Direct observations of the specific resistance of individual Cu grain boundaries has been achieved using four-point probe transport measurements with conducting scanning probe microscopy tips which detect discrete potential jumps $\Delta V =$ $(I/G_0A) \times r/(1-r)$ when moving across a grain boundary. G_0 is the specific ballistic conductance and I is the current flowing through a wire with a cross-sectional area A. ^{55–58} We note, r is here the reflection probability at one specific measured boundary, and is different at boundaries with different orientations and relative grain tilts. In contrast, R in Eq.(1) represents an effective mean probability for all boundaries (with different r) in a specimen. First-principles calculations have been used to determine the reflection probability at specific high-symmetry grain boundaries for a variety of metals including Cu, ^{44,59-61} Al, ⁶² W, ⁶³ Pt, Rh, Ir and Pd. ⁶⁴ Such calculations typically use coincidence site lattice (CSL) grain boundaries which are defined by the lattice sites that are shared by two periodic lattices which are rotated with respect to each other. Most frequently studied are the twin boundaries $\Sigma 3$, $\Sigma 5$, $\Sigma 9$ and $\Sigma 11$ where the Σ value corresponds to the inverse of the coincidence site density. 44,59-61,64 These symmetric boundaries have a relatively low boundary energy and are therefore commonly found in Cu interconnects and other FCC crystals. 56,59,60 We propose that their calculated r can be used as a benchmark to compare the grain boundary reflection of different metals. Thus, in this work, we use first-principles calculations to predict r at $\Sigma 3$, $\Sigma 5$, $\Sigma 9$ and $\Sigma 11$ grain boundaries of the most conductive fcc metals, namely Cu, Ag, Au, Al, Ca, Ni, Rh and Ir. We also provide a first order approximation of their random grain boundary reflection probability r_r by extrapolation from the four calculated specific r values, yielding the benchmark quantity $\rho_0 \lambda \times r_r / (1-r_r)$ for direct metal comparison.

Density functional theory calculations of CSL grain boundaries are carried out with the Quantum ESPRESSO package, 65,66 using a plain-wave basis set, the Perdew-Burke-Ernzerhof exchange correlation functional, 67 projector augmented wave pseudo potentials taken from the Quantum ESPRESSO PSlibrary, 68 k-point meshes with a spacing smaller than $0.05 \ 2\pi/a$ where a is the (conventional) lattice constant taken from the Virtual Nanolab database, and a Methfessel-Paxton smearing with a spreading value of $0.002 \ Ry$. Spin-polarization is not accounted for, which is expected to only affect the reliability of the results on Ni. Super cells containing two grain boundaries of the same kind are constructed in order to apply periodic boundary conditions for the self-consistent electronic structure and structural relaxation calculations. The length L of the super cell along the normal of the grain boundaries is four times the length of the unit vector in that crystallographic direction, with the two grain boundaries located at 0.25L and 0.75L. Each plane parallel to the grain boundaries contains one atom within the super cell. All atoms within a distance of a/2 away from the grain boundaries are relaxed from their original geometric positions, which are defined by the boundary type ($\Sigma 3$, $\Sigma 5$, $\Sigma 9$ or $\Sigma 11$) as described in previous literature. 59,63 Details on the atomic positions and schematics of the grain boundaries are provided as supplementary

material. Subsequent electron transport simulations use half of the super cell (containing one grain boundary) as the scattering region. They are done with the Complex Band Structure (CBS) approach implemented in the PWCOND package, 69,70 using a 60×60 two-dimensional k-point mesh to determine the transmission coefficient. Simulated systems consist of a scattering region with one grain boundary which is perpendicular to the transport direction and two electrodes which are semi-infinite bulk crystals oriented and positioned to perfectly match the lattice in the scattering region on either side of the grain boundary. The reflection probability $r = 1 - T/T_0$ is obtained from the calculated transmission coefficient T of the scattering region which contains grain boundaries and the coefficient T_0 for defect-free electrodes.

Table 1 lists the calculated electron reflection probabilities at four twin grain boundaries Σ 3, Σ 5, Σ 9 and Σ 11 for the eight most conductive fcc metals Cu, Ag, Au, Al, Ca, Ni, Rh and Ir. Evidently, r varies considerably as a function of the grain boundary type for any given metal as well as between different metals, ranging from 0.01 for the Σ 3 twin boundary in Ag to 0.55 for the Σ9 boundary in Ni. The values for Cu, Ag, Al, Rh, and Ir can be directly compared to previously published first-principles predictions. 41,56,59,62,64 which use a range of computational methods and software packages including the NANODSIM, VASP, Atomistix, or QuantumATK packages employing various basis sets, atomic relaxation approaches and the non-equilibrium Green's function (NEGF) or Boltzmann transport methods to determine r. Our values in Table 1 overall agree with those from previous studies, with average absolute deviations in r of 0.04 for Cu, 41,56,59,64 0.03 for Ag, 41 0.07 for Al, 62 0.06 or Rh, 64 and 0.05 for Ir. 64 We attribute the deviations to the diverse computational approaches, approximations, and unit cell sizes leading to an estimated computational uncertainty of 5% in the calculated transmission coefficients. The reported r is obtained from the difference between two transmission coefficients, such that the relative uncertainty can become large for boundaries with small r, particularly the $\Sigma 3$ boundaries in Cu and Ag. However, independent of some remaining computational uncertainty, the data in Table 1 is well suited for direct quantitative comparison of different fcc metals since all values are calculated with the same approach.

Figure 1 is a plot of the data from Table 1. It is the electron reflection probability at $\Sigma 3$, $\Sigma 5$, Σ 9 and Σ 11 twin boundaries for the eight most conductive fcc metals Cu, Ag, Au, Al, Ca, Ni, Rh and Ir, as labeled. The x-axis in this plot is the inverse of the distance d between atomic planes parallel to the grain boundary, scaled by the lattice constant a of the conventional unit cell, as discussed below. The plot shows that for a given boundary type, the r value is similar for Cu, Ag, and Au, but is considerably (2-3×) larger for the other five metals. That is, elements from column 11 have larger boundary transmission probabilities than the other investigated fcc metals. This may be attributed to the s-character of the bands that cross the Fermi level in Cu, Ag, and Au, resulting in a relatively weak ionic potential and a correspondingly small electron scattering crosssection at displaced atoms at the boundary. Alternatively, the relatively spherical Fermi surfaces for Cu, Ag and Au is expected to result in a high chance for an electron that traverses the boundary to find an empty state with the same momentum in the neighboring grain, yielding a high transmission probability.³² Secondly, we note that r values of $\Sigma 5$ and $\Sigma 9$ boundaries are larger than of $\Sigma 3$ and $\Sigma 11$ boundaries for most investigated metals. This is attributed to additional atomic planes formed by the face centered atoms for $\Sigma 5$ and $\Sigma 9$ boundaries, effectively leading to a smaller interplanar distance d and an increased perturbation at the boundary. Correspondingly, we sort the four boundaries in the order $\Sigma 3$, $\Sigma 11$, $\Sigma 5$ and $\Sigma 9$ by ranking them according to a decreasing d=

 $\sqrt{3}/3$ a, $\sqrt{11}/11$ a, $\sqrt{5}/10$ a and 1/6 a, respectively, where a is the conventional FCC lattice constant. These arguments motivate the reciprocal "1/d" x-axis in the plot.

The data indicates an increasing reflection probability with a decreasing interplanar spacing, which is attributed to an increasing perturbation of atomic positions near the grain boundary. More specifically, the investigated twin boundaries can be defined by two crystals that are separated by a mirror plane: {111} for $\Sigma 3$, {120} for $\Sigma 5$, {221} for $\Sigma 9$ and {113} for $\Sigma 11$, as also shown in the supplementary material. Prior to atomic relaxation, the crystals are perfect on both sides of the mirror plane. However, the interatomic spacing between atoms from opposite sides deviates from that of the perfect crystal, resulting in a net force on atoms near the boundary which is expected to be inverse proportional to their distance. The smallest distance between two atoms on opposite sides is 2d and, correspondingly, the force is proportional to 1/d. Thus, we propose a functional form for the resulting atomic displacement of $\sqrt{2}a/\{4(1+dc)\}$ where the proportionality constant c relates the original interatomic distance to the displacement force and the prefactor $\sqrt{2}a/4$ is half of the nearest-neighbor distance in fcc crystals which is the expected maximum displacement. The displacement causes a potential perturbation \hat{V} which results in electron scattering and a corresponding reflection probability at the boundary:

$$r = 1 - \frac{1}{1 + \beta \hat{V}}.\tag{2}$$

Here β is a constant that relates the potential perturbation to electron scattering. We expect \hat{V} to be proportional to the square of the atomic displacement. Using the above functional form and this square proportionality yields after some rearrangement:

$$r = \frac{1}{1 + (\frac{1}{r_r} - 1)(1 + cd)^2}. (3)$$

Here the constant r_r is the reflection in the limit $d \to 0$, which corresponds to a *random* grain boundary with Miller indices that are so large that there is no significant in-plane periodicity.

The dashed curves in Fig. 1 are obtained by data fitting using Eq. (3). More specifically, we fit the data for Cu with two free fitting parameters: r_r and c. This yields $r_r = 0.27$ and c = 2.6. The former value is close to the reported effective mean grain boundary reflection probability R =0.30 for Cu, as determined from the measured resistivity and data fitting using the MS model.²⁴ This good agreement suggests that the experimentally measured average reflection at Cu grain boundaries matches the reflection probability r_r for a random grain boundary in Cu. However, we note that there is considerable data scattering in Fig. 1 and, as a consequence, other value pairs for the two fitting parameters yield similar fit qualities. For example, $r_r = 0.30$ and c = 3.1 yields a slightly steeper curve with a similar fit-quality with a χ^2 that is only 1% larger than for the case above, indicating considerable correlation of the two fitting parameters. Thus, in order to minimize ambiguity and quantitatively compare the data from the different metals, the geometric parameter c = 3.1 is kept fixed for all metals, while the material property r_r becomes the single fitting parameter. This yields the dashed lines in Fig. 1 and r_r values for each investigated metal. We note that the derivation of Eq. (3) is somewhat speculative and fixing c = 3.1 to obtain $r_r = 0.3$ for Cu is semi-arbitrary. However, the relative metal "ranking" in this study is unaffected by the exact functional form of Eq. (3) and even a simple linear fit of the data in Fig. 1 yields r_r values that match those reported in this paper with a maximum deviation of only 2%.

Table 2 lists the grain boundary reflection coefficient r_r for random grain boundaries determined using Eq. (3) and the data in Fig. 1. Only Ag has a r_r that is comparable to that of Cu, while most other fcc metals (Ca, Al, Ni, Rh, Ir) exhibit approximately two times larger values. This affects the resistivity contribution from random grain boundaries as evaluated using the previously reported $\rho_o \lambda$ values^{30,31} and the approximate expression from the MS model $\rho_{\rm gb} = 1.5 \times \rho_o \lambda / D \times R/(1-R)$ where we set $R = r_r$ to determine the quantity $\rho_o \lambda \times r_r/(1-r_r)$ for the eight metals, as listed in Table 2. This quantity represents the descriptor to benchmark materials according to their conductivity in the limit of a small but fixed average grain size D. Copper has the smallest value of $2.9 \times 10^{-16} \Omega m^2$, indicating the highest conductivity of all eight investigated metals in the limit of small randomly oriented grains. The value for Ag is 15% larger, which is attributed to the larger prefactor $\rho_o \lambda$. All other investigated metals have $\rho_o \lambda \times r_r/(1-r_r)$ products which are considerably larger than for Cu, by approximately a factor of two for Au and Rh, a factor of three for Al and Ir, and factors of four and six for Ni and Ca.

These results suggest that no fcc metal provides a conductivity advantage over copper in the limit where electron grain boundary scattering is the dominant resistivity contribution, since Cu shows the smallest predicted resistivity size effect. We note that this is in contrast to previous studies 32,39,71 which only focus on the $\rho_0\lambda$ product as benchmark metrics and correspondingly predict that Rh and Ir, and theoretically even Al, have the potential to outperform the conductivity of Cu in the limit of narrow lines. In that context we need to reiterate the two key conditions for which the calculated $\rho_0 \lambda \times r_r/(1-r_r)$ is an appropriate materials benchmark: (1) The average grain size is small $(D < \lambda)$ and D < d) such that ρ_{gb} is the dominant resistivity contribution. Conversely, bulk electron scattering dominates over grain boundary scattering if the grain size is comparable or larger than the bulk electron mean free path λ and, similarly, surface scattering dominates over grain boundary scattering if the grain size is comparable or larger than the wire width d. (2) Grains and boundaries are randomly oriented. Conversely, textured microstructures may result in r values that are well below the extrapolated r_r for random orientations. In addition, annealing of metallic samples may lead to microstructures which exhibit primarily low-energy grain boundaries that tend to be high-symmetry boundaries with small r values, 42,59,64,72 leading to experimental samples where $R < r_r$, and therefore a $\rho_{\rm gb}$ that is smaller than predicted.

In summary, first-principles predictions of the electron reflection probability r at high symmetry $\Sigma 3$, $\Sigma 5$, $\Sigma 9$ and $\Sigma 11$ grain boundaries in the eight most conductive fcc metals suggest that r increases with a decreasing interplanar spacing parallel to the boundary. This correlation is used to quantitatively compare the eight metals and predict their reflection coefficient r_r at random grain boundaries. Cu, Ag, and Au have an approximately two times smaller predicted r_r than the other fcc metals, which is attributed to the nearly spherical Fermi surface for elements of column 11. In the limit of small, randomly oriented grains, the resistivity is dominated by the contribution from electron scattering at grain boundaries and is proportional to the product $\rho_0 \lambda \times r_r/(1-r_r)$. This quantity is smaller for Cu than for all other investigated metals, suggesting that Cu conducts the best in the limit of small, randomly oriented grains with fixed size. Correspondingly, fcc metals that are considered as replacement for Cu in narrow interconnect lines are expected to only provide a conductance benefit if their microstructure minimizes the resistivity contribution from grain boundary scattering. This may be achieved by either (1) a grain size that is comparable or larger than the line width or (2) high-symmetry grain boundaries with an effective mean reflection probability R that is significantly smaller than r_r . The latter may be realized with textured microstructures and/or processing that favors low-energy low-resistivity boundaries.

ACKNOWLEDGMENTS

The authors acknowledge funding from SRC under task Nos. 2966, 3085, and 3115, the NY State Empire State Development's Division of Science, Technology and Innovation (NYSTAR) through Focus Center-NY–RPI Contract C180117, and the NSF under grant No. 1712752. Computational resources were provided by the Center for Computational Innovations at RPI.

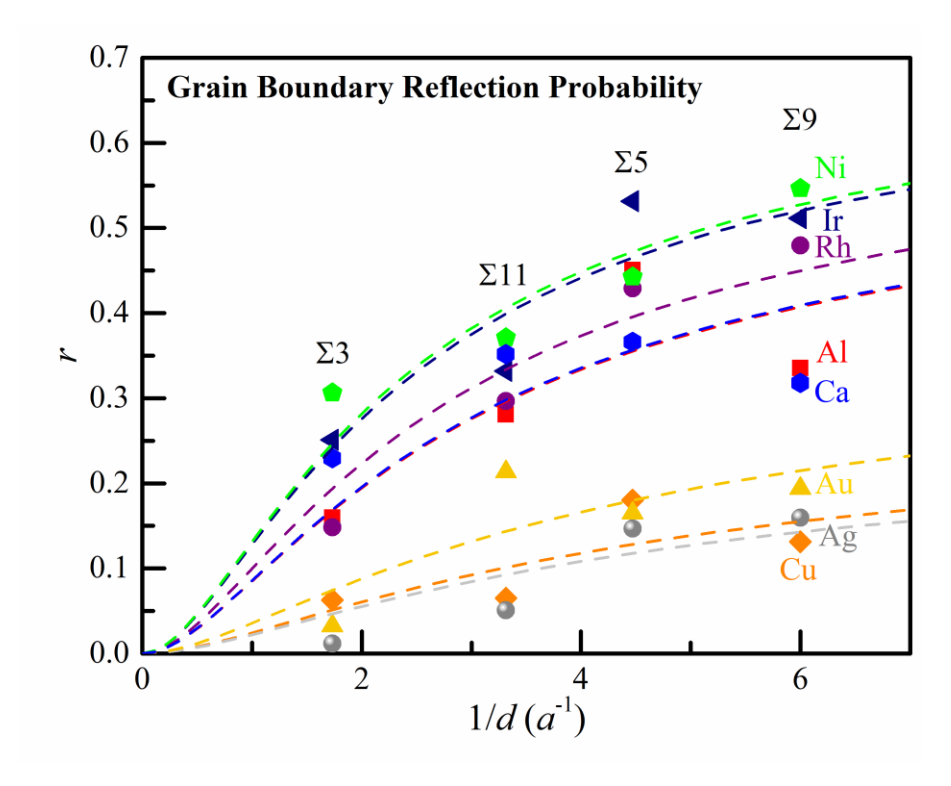


Figure 1: Calculated electron reflection probability r at $\Sigma 3$, $\Sigma 5$, $\Sigma 9$ and $\Sigma 11$ twin grain boundaries for eight fcc metals. The x-axis is the inverse of the interplanar distance d for planes parallel to the grain boundary in units of the reciprocal lattice constant a. The dotted lines are from data fitting using equation (3).

Table 1: Predicted electron reflection probability r at $\Sigma 3$, $\Sigma 5$, $\Sigma 9$ and $\Sigma 11$ coincidence grain boundaries for the eight most conductive fcc metals.

metal	Σ3	Σ5	Σ9	Σ11
Cu	0.06	0.18	0.13	0.07
Ag	0.01	0.15	0.16	0.05
Au	0.03	0.16	0.19	0.21
Al	0.16	0.45	0.34	0.28
Ca	0.23	0.37	0.32	0.35
Ni	0.31	0.44	0.55	0.37
Rh	0.15	0.43	0.48	0.30
Ir	0.25	0.53	0.51	0.33

Table 2: Predicted random grain boundary reflection probability r_r , product $\rho_o \lambda$ taken from Ref. 30, and benchmark material quantity $\rho_o \lambda \times r_r / (1 - r_r)$ for eight fcc metals.

metal	r_r	$ ho_{\omega}\lambda \ (10^{-16}~\Omega\mathrm{m}^2)$	$\rho_{\circ}\lambda\times[r_r/(1-r_r)]$ $(10^{-16}\ \Omega\text{m}^2)$
Cu	0.30	6.70	2.9
Ag	0.28	8.46	3.3
Au	0.39	8.35	5.3
Al	0.61	5.01	8.0
Ca	0.62	11.9	19.1
Ni	0.72	4.07	10.5
Rh	0.65	3.23	6.1
Ir	0.72	3.69	9.3

References

- ¹ W. Steinhögl, G. Schindler, G. Steinlesberger, and M. Engelhardt, Phys. Rev. B **66**, 075414 (2002).
- ² S.M. Rossnagel and T.S. Kuan, J. Vac. Sci. Technol. B Microelectron. Nanom. Struct. **22**, 240 (2004).
- ³ D. Josell, S.H. Brongersma, and Z. Tőkei, Annu. Rev. Mater. Res. **39**, 231 (2009).
- ⁴ R.C. Munoz and C. Arenas, Appl. Phys. Rev. **4**, 011102 (2017).
- ⁵ K. Fuchs, Math. Proc. Cambridge Philos. Soc. **34**, 100 (1938).
- ⁶ E.H. Sondheimer, Adv. Phys. **1**, 1 (1952).
- ⁷ A.F. Mayadas and M. Shatzkes, Phys. Rev. B **1**, 1382 (1970).
- ⁸ Z. Tešanović, M. V. Jarić, and S. Maekawa, Phys. Rev. Lett. **57**, 2760 (1986).
- ⁹ J.J. Plombon, E. Andideh, V.M. Dubin, and J. Maiz, Appl. Phys. Lett. **89**, 113124 (2006).
- ¹⁰ R.L. Graham, G.B. Alers, T. Mountsier, N. Shamma, S. Dhuey, S. Cabrini, R.H. Geiss, D.T. Read, and S. Peddeti, Appl. Phys. Lett. **96**, 042116 (2010).
- ¹¹ Y.P. Timalsina, X. Shen, G. Boruchowitz, Z. Fu, G. Qian, M. Yamaguchi, G.-C. Wang, K.M. Lewis, and T.-M. Lu, Appl. Phys. Lett. **103**, 191602 (2013).
- ¹² P. Zheng and D. Gall, J. Appl. Phys. **122**, 135301 (2017).
- ¹³ T. Zhou and D. Gall, Phys. Rev. B **97**, 165406 (2018).
- ¹⁴ T. Zhou, P. Zheng, S.C. Pandey, R. Sundararaman, and D. Gall, J. Appl. Phys. **123**, 155107 (2018).
- 15 K. Moors, B. Sorée, and W. Magnus, Microelectron. Eng. 167, 37 (2017).
- ¹⁶ D. Gall, J.J. Cha, Z. Chen, H. Han, C. Hinkle, J.A. Robinson, R. Sundararaman, and R. Torsi, MRS Bull. **46**, 959 (2021).
- ¹⁷ J.S. Chawla and D. Gall, Appl. Phys. Lett. **94**, 252101 (2009).
- ¹⁸ J.S. Chawla, F. Zahid, H. Guo, and D. Gall, Appl. Phys. Lett. **97**, 132106 (2010).
- ¹⁹ P.Y. Zheng, R.P. Deng, and D. Gall, Appl. Phys. Lett. **105**, 131603 (2014).
- ²⁰ P. Zheng, T. Zhou, and D. Gall, Semicond. Sci. Technol. **31**, 055005 (2016).
- ²¹ Y.P. Timalsina, A. Horning, R.F. Spivey, K.M. Lewis, T.-S. Kuan, G.-C. Wang, and T.-M. Lu, Nanotechnology **26**, 075704 (2015).
- ²² P.Y. Zheng, T. Zhou, B.J. Engler, J.S. Chawla, R. Hull, and D. Gall, J. Appl. Phys. **122**, 095304 (2017).
- ²³ E. Milosevic, S. Kerdsongpanya, A. Zangiabadi, K. Barmak, K.R. Coffey, and D. Gall, J. Appl. Phys. **124**, 165105 (2018).
- ²⁴ J.S. Chawla, F. Gstrein, K.P. O'Brien, J.S. Clarke, and D. Gall, Phys. Rev. B **84**, 235423 (2011).
- ²⁵ J.M. Rickman and K. Barmak, J. Appl. Phys. **114**, 133703 (2013).
- ²⁶ K. Barmak, A. Darbal, K.J. Ganesh, P.J. Ferreira, J.M. Rickman, T. Sun, B. Yao, A.P. Warren, and K.R. Coffey, J. Vac. Sci. Technol. A Vacuum, Surfaces, Film. **32**, 061503 (2014).
- ²⁷ G. Hegde, R.C. Bowen, and M.S. Rodder, in 2016 IEEE Int. Interconnect Technol. Conf. / Adv. Met. Conf. (IEEE, 2016), pp. 114–116.
- ²⁸ K. Moors, B. Soree, Z. Tokei, and W. Magnus, in *EUROSOI-ULIS 2015 2015 Jt. Int. EUROSOI Work. Int. Conf. Ultim. Integr. Silicon* (IEEE, 2015), pp. 201–204.
- ²⁹ G. Hegde, R.C. Bowen, and M.S. Rodder, Appl. Phys. Lett. **109**, 193106 (2016).
- ³⁰ D. Gall, J. Appl. Phys. **119**, 085101 (2016).
- ³¹ D. Gall, in 2018 IEEE Int. Interconnect Technol. Conf. (IEEE, 2018), pp. 157–159.
- ³² D. Gall, J. Appl. Phys. **127**, 050901 (2020).

- ³³ S. Dutta, K. Sankaran, K. Moors, G. Pourtois, S. Van Elshocht, J. Bömmels, W. Vandervorst, Z. Tőkei, and C. Adelmann, J. Appl. Phys. 122, 025107 (2017).
- ³⁴ K. Croes, C. Adelmann, C.J. Wilson, H. Zahedmanesh, O.V. Pedreira, C. Wu, A. Lesniewska, H. Oprins, S. Beyne, I. Ciofi, D. Kocaay, M. Stucchi, and Z. Tokei, Tech. Dig. - Int. Electron Devices Meet. IEDM 2018-Decem, 5.3.1 (2019).
- ³⁵ A. Jog and D. Gall, J. Appl. Phys. **130**, 115103 (2021).
- ³⁶ A. Jog, T. Zhou, and D. Gall, IEEE Trans. Electron Devices **68**, 257 (2021).
- ³⁷ K. Barmak, S. Ezzat, R. Gusley, A. Jog, S. Kerdsongpanya, A. Khanya, E. Milosevic, W. Richardson, K. Sentosun, A. Zangiabadi, D. Gall, W.E. Kaden, E.R. Mucciolo, P.K. Schelling, A.C. West, and K.R. Coffey, J. Vac. Sci. Technol. A Vacuum, Surfaces Film. 38, (2020).
- ³⁸ D. Gall, A. Jog, and T. Zhou, in 2020 IEEE Int. Electron Devices Meet. (IEEE, 2020), pp. 32.3.1-32.3.4.
- ³⁹ C. Adelmann, K. Sankaran, S. Dutta, A. Gupta, S. Kundu, G. Jamieson, K. Moors, N. Pinna, I. Ciofi, S. Van Eishocht, J. Bommels, G. Boccardi, C.J. Wilson, G. Pourtois, and Z. Tokei, in 2018 IEEE Int. Interconnect Technol. Conf. (IEEE, 2018), pp. 154–156.
- ⁴⁰ H. Bishara, S. Lee, T. Brink, M. Ghidelli, and G. Dehm, ACS Nano **15**, 16607 (2021).
- ⁴¹ B. Feldman, S. Park, M. Haverty, S. Shankar, and S.T. Dunham, Phys. Status Solidi **247**, 1791 (2010).
- ⁴² C. Arenas, G. Herrera, E. Muñoz, and R.C. Munoz, Mater. Res. Express 8, 015026 (2021).
- ⁴³ D. Valencia, E. Wilson, Z. Jiang, G.A. Valencia-Zapata, K.C. Wang, G. Klimeck, and M. Povolotskyi, Phys. Rev. Appl. 9, 44005 (2018).
- ⁴⁴ J. Lee, M. Lamarche, and V.P. Georgiev, 2018 IEEE 13th Nanotechnol. Mater. Devices Conf. NMDC 2018 1 (2019).
- ⁴⁵ J.M. Roberts, A.P. Kaushik, and J.S. Clarke, in 2015 IEEE Int. Interconnect Technol. Conf. 2015 IEEE Mater. Adv. Met. Conf. (IEEE, 2015), pp. 341–344.
- ⁴⁶ Y. Kaneno and T. Takasugi, Metall. Mater. Trans. A **34**, 2429 (2003).
- ⁴⁷ V. Randle, G.S. Rohrer, H.M. Miller, M. Coleman, and G.T. Owen, Acta Mater. **56**, 2363 (2008).
- ⁴⁸ K.J. Al-Fadhalah, J. Eng. Mater. Technol. Trans. ASME **134**, 1 (2012).
- ⁴⁹ T. Sun, B. Yao, A.P. Warren, V. Kumar, S. Roberts, K. Barmak, and K.R. Coffey, J. Vac. Sci. Technol. A Vacuum, Surfaces, Film. 26, 605 (2008).
- ⁵⁰ T. Sun, B. Yao, A.P. Warren, K. Barmak, M.F. Toney, R.E. Peale, and K.R. Coffey, Phys. Rev. B 79, 041402 (2009).
- ⁵¹ T. Sun, B. Yao, A.P. Warren, K. Barmak, M.F. Toney, R.E. Peale, and K.R. Coffey, Phys. Rev. B 81, 155454 (2010).
- ⁵² D. Choi, X. Liu, P.K. Schelling, K.R. Coffey, and K. Barmak, J. Appl. Phys. **115**, 104308
- (2014). ⁵³ I. Bakonyi, V.A. Isnaini, T. Kolonits, Z. Czigány, J. Gubicza, L.K. Varga, E. Tóth-Kádár, L. Pogány, L. Péter, and H. Ebert, Philos. Mag. 99, 1139 (2019).
- ⁵⁴ I. Bakonyi, Accounting for the Resistivity Contribution of Grain Boundaries in Metals: Critical Analysis of Reported Experimental and Theoretical Data for Ni and Cu (Springer Berlin Heidelberg, 2021).
- ⁵⁵ Y. Kitaoka, T. Tono, S. Yoshimoto, T. Hirahara, S. Hasegawa, and T. Ohba, Appl. Phys. Lett. **95**, 1 (2009).
- ⁵⁶ T.-H. Kim, X.-G. Zhang, D.M. Nicholson, B.M. Evans, N.S. Kulkarni, B. Radhakrishnan, E.A. Kenik, and A.-P. Li, Nano Lett. 10, 3096 (2010).

- ⁵⁷ H. Bishara, M. Ghidelli, and G. Dehm, ACS Appl. Electron. Mater. **2**, 2049 (2020).
- ⁵⁸ A.-P. Li, K.W. Clark, X.-G. Zhang, and A.P. Baddorf, Adv. Funct. Mater. **23**, 2509 (2013).
- ⁵⁹ M. César, D. Liu, D. Gall, and H. Guo, Phys. Rev. Appl. **2**, 044007 (2014).
- ⁶⁰ M. César, D. Gall, and H. Guo, Phys. Rev. Appl. **5**, 054018 (2016).
- ⁶¹ D. Valencia, E. Wilson, P. Sarangapani, G.A. Valencia-Zapata, G. Klimeck, M. Povolotskyi, and Z. Jiang, Int. Conf. Simul. Semicond. Process. Devices, SISPAD 105 (2016).
- 62 T. Zhou, N.A. Lanzillo, P. Bhosale, D. Gall, and R. Quon, AIP Adv. 8, 055127 (2018).
- ⁶³ N.A. Lanzillo, H. Dixit, E. Milosevic, C. Niu, A. V. Carr, P. Oldiges, M. V. Raymond, J. Cho, T.E. Standaert, and V.K. Kamineni, J. Appl. Phys. **123**, 154303 (2018).
- ⁶⁴ N.A. Lanzillo, J. Appl. Phys. **121**, 175104 (2017).
- ⁶⁵ P. Giannozzi, S. Baroni, N. Bonini, M. Calandra, R. Car, C. Cavazzoni, D. Ceresoli, G.L. Chiarotti, M. Cococcioni, I. Dabo, A. Dal Corso, S. de Gironcoli, S. Fabris, G. Fratesi, R. Gebauer, U. Gerstmann, C. Gougoussis, A. Kokalj, M. Lazzeri, L. Martin-Samos, N. Marzari, F. Mauri, R. Mazzarello, S. Paolini, A. Pasquarello, L. Paulatto, C. Sbraccia, S. Scandolo, G. Sclauzero, A.P. Seitsonen, A. Smogunov, P. Umari, and R.M. Wentzcovitch, J. Phys. Condens. Matter 21, 395502 (2009).
- ⁶⁶ P. Giannozzi, O. Andreussi, T. Brumme, O. Bunau, M. Buongiorno Nardelli, M. Calandra, R. Car, C. Cavazzoni, D. Ceresoli, M. Cococcioni, N. Colonna, I. Carnimeo, A. Dal Corso, S. de Gironcoli, P. Delugas, R.A. DiStasio, A. Ferretti, A. Floris, G. Fratesi, G. Fugallo, R. Gebauer, U. Gerstmann, F. Giustino, T. Gorni, J. Jia, M. Kawamura, H.-Y. Ko, A. Kokalj, E. Küçükbenli, M. Lazzeri, M. Marsili, N. Marzari, F. Mauri, N.L. Nguyen, H.-V. Nguyen, A. Otero-de-la-Roza, L. Paulatto, S. Poncé, D. Rocca, R. Sabatini, B. Santra, M. Schlipf, A.P. Seitsonen, A. Smogunov, I. Timrov, T. Thonhauser, P. Umari, N. Vast, X. Wu, and S. Baroni, J. Phys. Condens. Matter 29, 465901 (2017).
- ⁶⁷ J.P. Perdew, K. Burke, and M. Ernzerhof, Phys. Rev. Lett. **77**, 3865 (1996).
- ⁶⁸ G. Prandini, A. Marrazzo, I.E. Castelli, N. Mounet, and N. Marzari, Npj Comput. Mater. **4**, 72 (2018).
- ⁶⁹ H. Joon Choi and J. Ihm, Phys. Rev. B Condens. Matter Mater. Phys. **59**, 2267 (1999).
- ⁷⁰ A. Smogunov, A. Dal Corso, and E. Tosatti, Phys. Rev. B **70**, 045417 (2004).
- ⁷¹ A.J. Simbeck, N. Lanzillo, N. Kharche, M.J. Verstraete, and S.K. Nayak, ACS Nano **6**, 10449 (2012).
- ⁷² N. V. Doubina, T.A. Spurlin, E.C. Opocensky, and J.D. Reid, MRS Adv. 5, 1919 (2020).